

Rydberg hydrogen atom near a metallic surface: Stark regime and ionization dynamics

Manuel Iñarraea,^{1,*} Víctor Lanchares,² Jesús F. Palacián,³ Ana Isabel Pascual,² J. Pablo Salas,^{1,†} and Patricia Yanguas³

¹*Área de Física Aplicada, Universidad de La Rioja, Logroño, Spain*

²*Departamento de Matemáticas y Computación, Universidad de La Rioja, Logroño, Spain*

³*Departamento de Ingeniería Matemática e Informática, Universidad Pública de Navarra, Pamplona, Spain*

(Received 20 July 2007; published 21 November 2007)

We investigate the classical dynamics of a hydrogen atom near a metallic surface in the presence of a uniform electric field. To describe the atom-surface interaction we use a simple electrostatic image model. Owing to the axial symmetry of the system, the z -component of the canonical angular momentum P_ϕ is an integral and the electronic dynamics is modeled by a two degrees of freedom Hamiltonian in cylindrical coordinates. The structure and evolution of the phase space as a function of the electric field strength is explored extensively by means of numerical techniques of continuation of families of periodic orbits and Poincaré surfaces of section. We find that, due to the presence of the electric field, the atom is strongly polarized through two consecutive pitchfork bifurcations that strongly change the phase space structure. Finally, by means of the phase space transition state theory and the classical spectral theorem, the ionization dynamics of the atom is studied.

DOI: [10.1103/PhysRevA.76.052903](https://doi.org/10.1103/PhysRevA.76.052903)

PACS number(s): 34.50.Dy, 45.20.Jj, 34.10.+x, 82.20.Db

I. INTRODUCTION

When a slowly moving atom or ion approaches a metallic surface, the mutual interaction leads to electronic processes of great interest in physics (see, e.g., [1] and references therein). In particular, due to the large size of the atom and the weak binding of the excited electron, Rydberg atoms are especially sensitive to the perturbations induced by a nearby metal surface. In this sense, and even at large distances from the surface, image charge effects strongly distort the electronic states and reorganize the energy levels of the atom [2]. Moreover, as the atom approaches the surface, the outer electron is captured by the surface and the atom ionizes [3]. After this charge transfer process, the positive ion is attracted to the surface by its image charge and finally it is neutralized by an Auger process. A fundamental question involved in a charge transfer process is to determine how far from the metallic surface the ionization of the atom takes place, i.e., to know the ionization distance. In this sense, in most of the experiments, an external static electric field perpendicular to the surface is applied in such a way that, when the electric field is strong enough, its Coulombic force on the ion is able to counteract the metallic attraction. Then the ion escapes the surface providing an experimentally observable signal [4–8] that allows one to determine the distance to the surface where the atom ionizes.

Moreover, theoretical studies show that when the atom approaches the surface or when the electric field strength increases, before the ionization, the electron falls on a Stark-type regime in which some electronic wave functions are strongly oriented either toward or opposite to the surface [4,6,8]. This feature has been used in experiments to study the ionization of xenon Rydberg atoms near an Au(111) surface [7].

In practice, when the interaction with the metallic surface is described by a suitable mathematical model, the charge transfer process at hand can be included into the family of Rydberg atoms in external fields. It belongs to this family, for instance, the well-known problem of a Rydberg atom interacting with a strong magnetic field (the quadratic Zeeman effect) [9]. All members of this family share the property that quantum and classical worlds overlap with the result that classical mechanics is able to explain with astonishing accuracy many quantum properties [10].

At this point, and in the framework of classical mechanics, we study in this paper the dynamics of a Rydberg atom perturbed by an external static electric field and by a nearby metallic surface. In particular, because most of the theoretical studies have been done with hydrogen [2,11], we use this atom in our approach. With this atom choice the interaction of the Rydberg electron with the nucleus is purely Coulombic. Because the interactions with the metal surface take place relatively far from the surface, the surface-atom potential is assumed to be simple in form. Then for a hydrogen atom, an image model [2,11,12] is suitable. As we will see through the paper, our goal is twofold. On the one hand, we show that from a classical point of view, the Stark regime takes place through two consecutive pitchfork bifurcations. When the system reaches this regime, two rectilinear orbits are the backbone of the phase space. One of the orbits is oriented toward the surface while the other one is oriented to the vacuum. On the other hand, the ionization mechanics of the atom is explained by using the modern theory of phase space transition state [13]. Under this approach, we are able to obtain analytically the geometric structures that in phase space regulate the ionization of the atom as well as to calculate efficiently the ionization probability of the atom as a function of the electric field strength.

The paper is organized as follows. Section II is devoted to the posing of the problem. From the assumed image model, we manage a two degrees of freedom Hamiltonian system. We establish the relevant parameters controlling the dynamics and, by analyzing the critical points of the effective po-

*manuel.inarraea@unirioja.es

†josepablo.salas@unirioja.es

tential, we can understand part of the dynamics. In Sec. III, we study the evolution of the fundamental families of periodic orbits that determine the phase space structure. We find the bifurcations that lead to the Stark regime. In Sec. IV we use the phase space transition state theory to determine the geometric structures that govern the capture of the electron by the metallic surface. In Sec. V we use the results of the previous section and the classical spectral theorem of Pollak [15] to determine the ionization probability of the atom. The results are compared to a brute-force Monte Carlo calculation. Finally, in Sec. VI we summarize the results.

II. PROBLEM

Let us consider the motion of an electron in a Coulombic field induced by an infinitely massive nucleus of charge $e > 0$ at the origin of the coordinate system. The metallic surface is located at the plane $z = -d$ and an electric field of strength $F > 0$ along the z axis is superimposed. In cylindrical coordinates $(\rho, z, \phi, P_\rho, P_z, P_\phi)$ and atomic units (a.u.), the electronic Hamiltonian of the system is given by

$$\mathcal{H} = E = \frac{P_\rho^2 + P_z^2}{2} + \frac{P_\phi^2}{2\rho^2} - \frac{1}{\sqrt{\rho^2 + z^2}} + Fz + \frac{1}{\sqrt{\rho^2 + (2d+z)^2}} - \frac{1}{4(d+z)}, \quad (1)$$

where the last two terms account for the image model describing the interaction of the hydrogen atom with the metallic surface [12]. Owing to the axial symmetry, the z component P_ϕ of the angular momentum is conserved and Eq. (1) defines a two degree-of-freedom dynamical system. Besides P_ϕ and the energy E , the system depends on the external parameters d and F . Here in this paper we reduce ourselves to the case $P_\phi = 0$. At this point, it is useful to scale coordinates and momenta in the form

$$\mathbf{r}' = \mathbf{r}/d, \quad \mathbf{P}' = d^{1/2} \mathbf{P}.$$

After dropping primes, Hamiltonian (1) becomes

$$\mathcal{H}' = \mathcal{E} = E d = \frac{P_\rho^2 + P_z^2}{2} - \frac{1}{\sqrt{\rho^2 + z^2}} + \frac{1}{\sqrt{\rho^2 + (2+z)^2}} - \frac{1}{4(1+z)} + fz, \quad (2)$$

and the dynamics depends only on the scaled energy $\mathcal{E} = E d$ and on the scaled electric field $f = F d^2$. Then, by keeping \mathcal{E} and f constant and simultaneously changing E , F , and d , we can explore different regions where the classical dynamics remains invariant.

It is useful to study the shape of the effective potential $U(\rho, z)$ in Eq. (2),

$$U(\rho, z) = -\frac{1}{\sqrt{\rho^2 + z^2}} + \frac{1}{\sqrt{\rho^2 + (2+z)^2}} - \frac{1}{4(1+z)} + fz, \quad (3)$$

through the determination of its critical points, which are the roots of the equations $U_z = 0$ and $U_\rho = 0$,

$$U_z = \frac{\partial U(\rho, z)}{\partial z} = f + \frac{1}{4(1+z)^2} + \frac{z}{(\rho^2 + z^2)^{3/2}} - \frac{2+z}{[\rho^2 + (2+z)^2]^{3/2}} = 0,$$

$$U_\rho = \frac{\partial U(\rho, z)}{\partial \rho} = \frac{\rho}{(\rho^2 + z^2)^{3/2}} - \frac{\rho}{[\rho^2 + (2+z)^2]^{3/2}} = 0. \quad (4)$$

Due to the Coulombic term, the effective potential $U(\rho, z)$ shows an infinite potential well at the origin. The critical points $P_s = (\rho_s, z_s)$ of $U(\rho, z)$, when they exist, take place on the z axis ($\rho_s = 0$). By substituting $\rho_s = 0$ in Eq. (4), the values of z_s are the roots of the following equation:

$$\mathcal{Z}(z) = \mathcal{R}(z) - \mathcal{S}(z) = 0, \quad (5)$$

where \mathcal{R} and \mathcal{S} are

$$\mathcal{R}(z) = f + \frac{z}{|z|^3}, \quad \mathcal{S} = -\frac{1}{4(1+z)^2} + \frac{1}{(2+z)^2}. \quad (6)$$

The direct application of the Bolzano theorem as well as the increasing and decreasing behavior of \mathcal{R} and \mathcal{S} ensure that these functions intersect always once and only once in the interval $(-1, 0)$. Then the effective potential $U(\rho, z)$ presents a unique critical point $P_s = (0, z_s)$ in that interval. Moreover, z_s is the real root of the following polynomial equation arising from Eq. (5)

$$\mathcal{P}(z) = -16 - 48z + (-52 + 16f)z^2 + (-28 + 48f)z^3 + (-7 + 52f)z^4 + 24fz^5 + 4fz^6 = 0. \quad (7)$$

For $f = 0$, \mathcal{P} is a four-degree polynomial, and the analytic expression of z_s is given by

$$z_s = -1 + \sqrt{\frac{-5 + 4\sqrt{2}}{7}} \approx -0.693\ 673.$$

By substituting P_s in the corresponding Hessian matrix, we readily obtain that P_s is a saddle point whose energy is $\mathcal{E}_s \approx -1.492\ 218$. For $f \neq 0$, \mathcal{P} is a six-degree polynomial equation and it is not possible to obtain the analytic expression of z_s . However, we can express asymptotically the coordinate z_s in terms of f as

$$z_s(f) = -0.693673 + 0.044466f + 0.006259f^2 + 0.000220f^3 + \mathcal{O}(f^4)$$

From the above expression of z_s we deduce that, as f increases, z_s approaches zero. In Fig. 1 is depicted the behavior of $U(\rho, z)$ for two different values of f . Because $P_\phi = 0$, the orbital plane (ρ, z) is always perpendicular to the x - y plane. Then, although ρ is a cylindrical coordinate, in this case it can be considered as a Cartesian coordinate in the orbital plane with positive and negative values and it is more illustrative to plot the figures in coordinates $(\pm\rho, z)$. From a physical point of view, the saddle point P_s is the ionization channel through which the electron can be captured by the metallic surface.

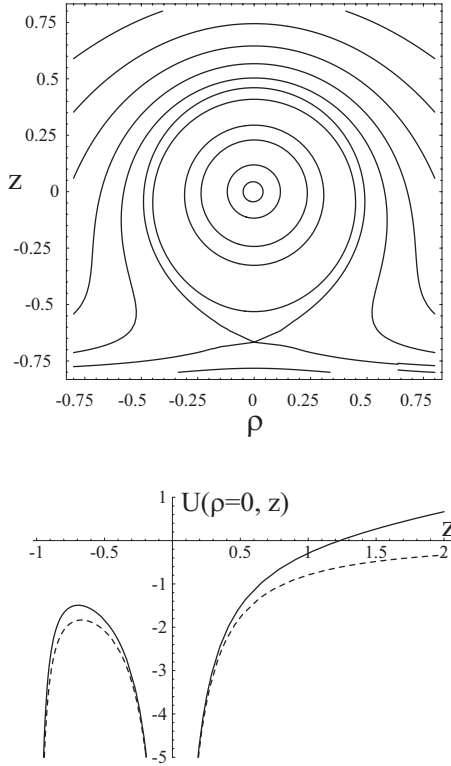


FIG. 1. Upper panel: Equipotential curves of the effective potential $U(\rho, z)$ for scaled electric field $f=0.5$. Lower panel: Effective potential $U(\rho, z)$ for $\rho=0$ and $f=0$ (solid line) and $f=0.5$ (dashed line).

III. PHASE SPACE STRUCTURE

In this section we are interested in the evolution of the phase space governed by the Hamiltonian (2) which depends on the parameters (\mathcal{E}, f) . The phase space structure is mainly characterized by the number and stability of the periodic orbits. Once a periodic orbit is calculated, the stability of that orbit can also be computed, which sheds light on the character of phase space in the vicinity of the orbit. The continuation of families of periodic orbits generated by variations of any of the system's parameters and the computation of the stability parameter of the family helps then in understanding the dynamics of the problem.

As it is well known, the linear stability of a periodic orbit is determined from the eigenvalues of the monodromy matrix. Since we are dealing with a Hamiltonian problem, the eigenvalues appear in reciprocal pairs, and as a consequence of the invariance of the Hamiltonian equations of motion we have one trivial eigenvalue $\lambda_0=1$ with multiplicity 2. Then, the stability index

$$k = \lambda + 1/\lambda \quad (8)$$

is normally used, where the condition k is real and $|k| < 2$ applies for linear stability, and the critical value $k = \pm 2$ means that a new family of periodic orbits has likely bifurcated from the original one. Therefore stability diagrams where the stability index is presented versus the parameter generator of the family are commonly used. Since we work

with a system of two degrees of freedom, the computation of Poincaré surfaces of section allows us to illustrate the phase space structure.

At this point, we proceed as follows: First, we fix a value of the parameter f for which periodic solutions exist in the phase space. Then, by using the numerical software AUTO [16] we carry out the numerical continuation of the families of periodic orbits—by varying one parameter, while the other remains constant—that emanate from those solutions. The stability diagram of every periodic orbit of each family as a function of the corresponding parameter is also computed. From this diagram, we can detect values of the parameter for which possible bifurcations take place. Bifurcations produce qualitative changes in the phase space structure. When a bifurcation is found, the study is completed by calculating the corresponding surfaces of section.

Moreover, because for $P_\phi=0$ there is no centrifugal barrier, the electron can reach the origin and then Hamiltonian (2) presents a singularity. To avoid the numerical problems involved with this singularity, we perform the so-called Levi-Civita regularization [17]. This procedure starts with a change to semiparabolic coordinates (u, v) ,

$$\rho = uv, \quad z = (u^2 - v^2)/2.$$

Next, we define a new scaled time $\tau = t/(u^2 + v^2)$. Finally, after an overall multiplication by $u^2 + v^2$, the Hamiltonian (2) reads

$$\begin{aligned} \hat{\mathcal{H}} = 2 = & \frac{P_u^2 + P_v^2}{2} - \mathcal{E}(u^2 + v^2) + \frac{2(u^2 + v^2)}{\sqrt{4u^2v^2 + (4 + u^2 - v^2)^2}} \\ & - \frac{u^2 + v^2}{2(2 + u^2 - v^2)} + \frac{f}{2}(u^4 - v^4). \end{aligned} \quad (9)$$

The Hamilton equations of motion arising from Eq. (9) are

$$\begin{aligned} \dot{u} = P_u, \quad \dot{P}_u = & u \left(2\mathcal{E} - 2fu^2 - \frac{2(-1 + v^2)}{(2 + u^2 - v^2)^2} \right. \\ & \left. - \frac{16(4 + u^2 - 3v^2)}{[u^4 + (-4 + v^2)^2 + 2u^2(4 + v^2)]^{3/2}} \right), \\ \dot{v} = P_v, \quad \dot{P}_v = & v \left(2\mathcal{E} + 2fv^2 + \frac{2(1 + u^2)}{(2 + u^2 - v^2)^2} \right. \\ & \left. - \frac{16(4 + 3u^2 - v^2)}{[u^4 + (-4 + v^2)^2 + 2u^2(4 + v^2)]^{3/2}} \right). \end{aligned} \quad (10)$$

In searching for particular solutions of Eq. (10), we find the following:

(1) Rectilinear orbits along the v axis ($u=0$) always exist. They correspond to rectilinear orbits along the negative z axis. For historical reasons, we name these orbits as I_∞^- .

(2) Rectilinear orbits along the u axis ($v=0$) always exist. They are named as I_∞^+ , and they correspond to rectilinear orbits along the positive z axis.

To get an overall vision of the phase space structure where the two particular solutions exist, we fix a value of $f=0$, extensively studied by Simonovic [18], and compute the surface of section by numerical integration of the equations

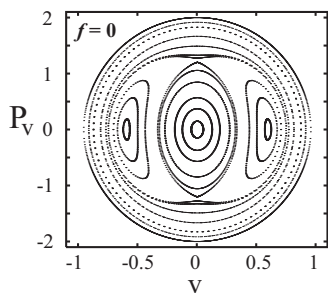


FIG. 2. Poincaré surface of section for scaled energy $\mathcal{E}=-2$ and scaled electric field $f=0$.

of motion (10). The surface of section is defined as the projection of the phase trajectories on the $u=0$ plane with $P_u \geq 0$. Under these conditions, the available region of the surface of section is limited by the curves

$$P_v = \pm \sqrt{4 + 2\mathcal{E}v^2 + fv^4 + \frac{v^2}{2-v^2} - \frac{4v^2}{\sqrt{16-8v^2+v^4}}}. \quad (11)$$

It is worth noting that rectilinear orbits I_∞^- are tangent to the flux in this Poincaré map and they correspond to the curves (11). To compute the surface of section, we fix $\mathcal{E}=-2$ because for this energy the electron is confined into the infinite potential well and its dynamics is still close to the integrable limit $\mathcal{E} \rightarrow -\infty$ [18]. The corresponding surface of section for $\mathcal{E}=-2$ is shown in Fig. 2 where we distinguish four important structures:

(i) The stable central fixed point $(0, 0)$ corresponds to the rectilinear orbit I_∞^+ . Hence the levels around this point are vibrational-type quasiperiodic orbits with the same symmetry patterns as I_∞^+ ; that is to say, mainly localized along the positive z axis. We name these levels as V_∞^+ .

(ii) The two stable fixed points symmetrically located on the v axis, named C , correspond to almost circular orbits traveling in opposite directions. When the energy $\mathcal{E} \ll 0$, they become circular with coordinates $(\pm 2/\sqrt{1-4\mathcal{E}}, 0)$. The levels around these points are rotational-type quasiperiodic orbits with the same symmetry patterns as C .

(iii) The above three regions are kept apart by a heteroclinic orbit (separatrix) passing through the two unstable (hyperbolic) fixed points located at the P_v axis. We name these points as H . When the energy $\mathcal{E} \ll 0$, these points H have coordinates $(0, \pm\sqrt{2})$ and they are unstable rectilinear orbits with coordinates $u=v$, that is to say, they correspond to rectilinear orbits along the ρ axis.

(iv) Finally, and taking into account that the limit of the surface of section is the rectilinear orbit I_∞^- , the levels above the separatrix H are vibrational quasiperiodic orbits mainly oriented along the negative z axis. These vibrational levels are denoted as V_∞^- . We note that, while the stability of the fixed points appearing inside the surface of section can be established at a glance, the stability of I_∞^- (the limit of the surface of section) must be determined by using the Index theorem. In this way, because the domain D of the surface of section is homeomorphic to a two-dimensional sphere, the

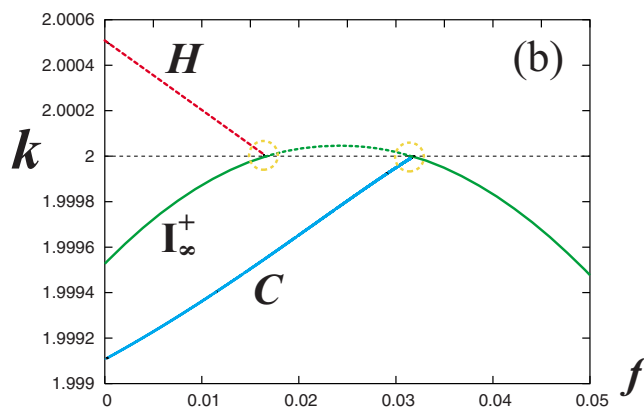
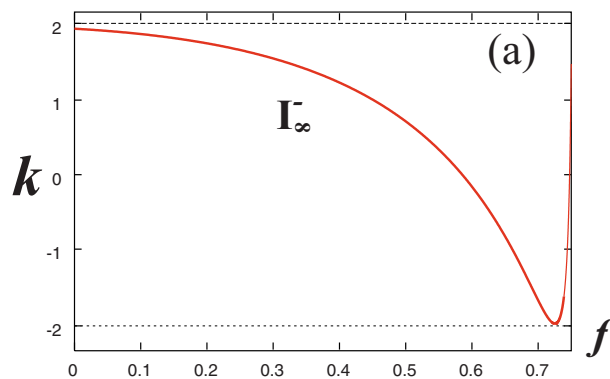


FIG. 3. (Color online) Stability diagram of the families of periodic orbits I_∞^- , I_∞^+ , C , and H as a function of the scaled electric field f . Dashed lines indicate instability.

sum of the indexes of the fixed points must be 2. Because the surface of section shows two unstable critical points (with index -1) and three stable fixed points (with index 1), the index of the periodic orbit I_∞^- must be 1 in order to keep fixed the Euler characteristic to 2 . Then, I_∞^- is a stable periodic orbit.

Note that, although the system is nonintegrable, all the phase orbits are confined to adiabatic invariant tori in accordance to a near integrable behavior. This is the expected result when the energy is smaller than the escape energy $\mathcal{E}_s(f=0)=-1.492\ 218$.

Therefore there are available four periodic orbits for $f=0$ from which we start the continuation procedure. For the fixed value $\mathcal{E}=-2$, we compute the family that emanates from each periodic orbit as f varies. The stability diagram of these families is shown in Fig. 3. This diagram gives the stability parameter k of each family in the interval $0 \leq f < f_s$, where $f_s \approx 0.751\ 391$ is the value at which the energy $\mathcal{E}=-2$ is equal to the saddle point energy \mathcal{E}_s . We call each family with the same name as the corresponding periodic orbit. The family I_∞^- is always stable [see Fig. 3(a)]. After a careful look to Fig. 3(b), we see that at the values $f_1 \approx 0.016\ 875$ and $f_2 \approx 0.031\ 875$ two consecutive bifurcations take place because in their vicinity the families H and C terminate on the positive z axis: First, the unstable family H at f_1 , and then the stable family C at f_2 . From $f > f_2$ to $f \approx f_s$, there are no more bifurcations.

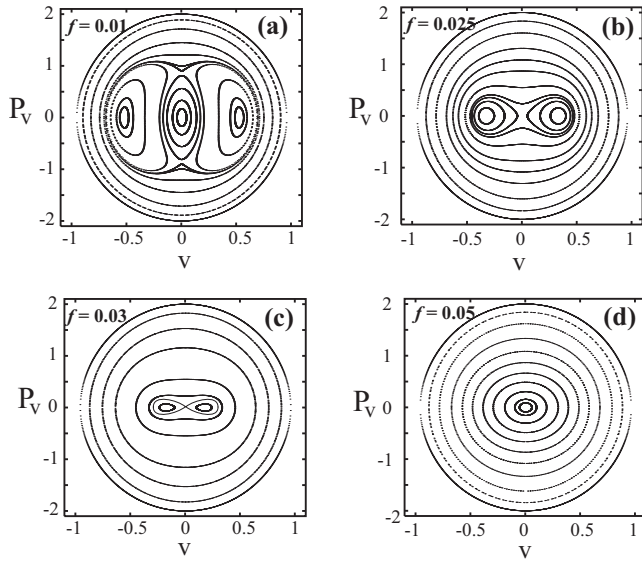


FIG. 4. Evolution of the Poincaré surfaces of section as a function of the scaled electric field f for scaled energy $\mathcal{E}=-2$.

The described behavior is easily visualized by computing surfaces of section for some convenient values of f ranging in the interval $0 < f < f_s$. For $f=0.01$ [see Fig. 4(a)] the surface of section presents the same qualitative structure as Fig. 2. However, due to the presence of the electric field, the unstable fixed points H moved toward the stable central point I_∞^+ . Then as we approach f_1 , the fixed points H become progressively periodic orbits along the positive z axis. Note that the fixed points C are also simultaneously moving along the v axis toward the fixed point I_∞^+ . When the electric field reaches the value f_1 , the collapse between the fixed points H and I_∞^+ occurs. From this collision, only I_∞^+ , which becomes unstable, survives [see Fig. 4(b)] and a pitchfork bifurcation takes place. As the electric parameter tends to f_2 , the fixed points C approach I_∞^+ [see Fig. 4(c)]. When $f=f_2$, a second pitchfork bifurcation occurs: C and I_∞^+ come into coincidence in such a way that only I_∞^+ survives, becoming stable [see Fig. 4(d)]. After this bifurcation the phase space is made of vibrational orbits and there is a smooth evolution from vibrational V_∞^+ to vibrational V_∞^- orbits: The nearer the orbit is to I_∞^+ (I_∞^-), the greater its orientation is along the positive (negative) z axis. In this way, from the second bifurcation, a Stark-type regime prevails. Roughly speaking, the electric field polarizes the atom along the z axis because the orbits are mainly oriented along the z direction.

It is worth noting that this classical Stark behavior has a quantum counterpart. Indeed, theoretical studies [5,6] have revealed that wave functions are strongly oriented along that direction. In particular, this fact can be observed in Fig. 4 of Ref. [6], where two opposite strongly oriented states are depicted for an applied electric field of $F=2.8 \times 10^{-6}$ a.u. and an atom-surface separation $d=670$ a.u. The parameters used in that figure correspond to scaled values $f \approx 1.3$ and $\mathcal{E} \approx -3.3$. When the surface of section with these scaled parameters is computed (see Fig. 5), we find that the classical phase space shows a clear Stark structure.

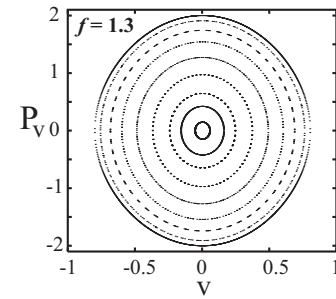


FIG. 5. Poincaré surface of section for scaled energy $\mathcal{E}=-3.3$ and scaled electric field $f=1.3$.

IV. IONIZATION DYNAMICS

When the energy \mathcal{E} of the electron is bigger than the escape energy \mathcal{E}_s , the electron has access to the ionization channel located along the negative z axis and can be captured by the metallic surface. In Fig. 6 two surfaces of section are shown for $\mathcal{E}=-2$ and for values of f for which $\mathcal{E}_s < \mathcal{E}=-2$. We note that, in regularized coordinates, the escape channel is located along the v axis in such a way that, when $\mathcal{E}_s < \mathcal{E}$ the surface of section is not a bounded region because the rectilinear orbit I_∞^- (the limit of the surface of section) is the first orbit to ionize. However, although $\mathcal{E} > \mathcal{E}_s$, not all trajectories escape because part of the phase space remains isolated from the ionization channel due to the presence of the

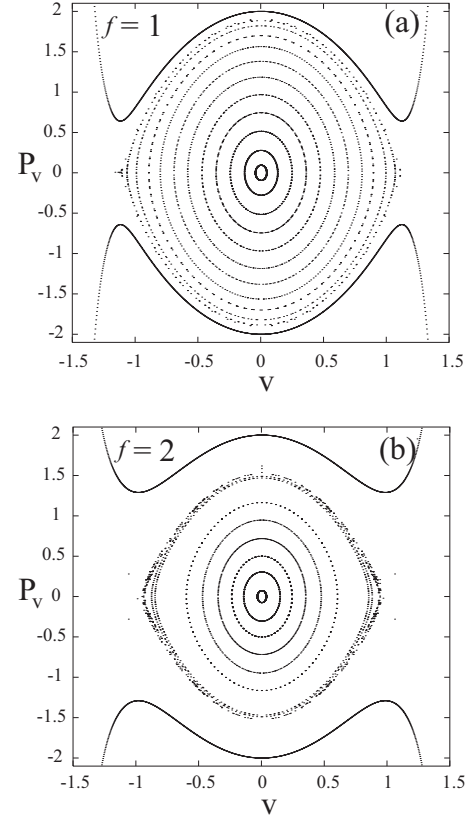


FIG. 6. Poincaré surfaces of section for scaled energy $\mathcal{E}=-2$ and for (a) $f=1$ and (b) $f=2$.

stability island around I_{∞}^+ . When f increases, more and more orbits have access to the ionization channel and the “hole” in the corresponding surface of section grows whereas the stability island around I_{∞}^+ becomes smaller [see Fig. 6(b)]. Hence the presence of the electric field increases the number of initial conditions that lead to escape and therefore the ionization probability grows.

A deeper understanding of the ionization of the atom is obtained when we face the problem from the point of view of chemical reaction dynamics. From this regard, to be captured by the metallic surface, the electron must overcome a potential energy barrier and this process resembles a chemical reaction. In reaction dynamics, the transition state theory [19] postulates the existence of a minimal set of states in phase-space, the transition state (TS), that all reactive trajectories cross and which is never encountered by nonreactive trajectories. In other words, there exists a dividing surface in phase-space that separates “reactants” from “products.” However, the problem of how to construct analytically the TS remained as an open question until Wiggins and co-workers [13,14] developed phase space transition state theory (PSTST). This theory is based on the new geometrical insights for nonlinear Hamiltonian systems and its main goal is to provide an algorithmic procedure to determine analytically the geometrical objects that separate “reactants” from “products.”

Moreover, the use of the PSTST together with a classical spectral theorem developed by Pollak in the 1970s [15] provide an elegant and very efficient way to calculate the phase space volume of initial conditions that give rise to escape trajectories. In the next section we apply this method to compute the ionization probability in our problem.

We start with some brief remarks on PSTST. Let us consider a generic n -degrees of freedom Hamiltonian $\mathcal{H}(x_1, \dots, x_n, p_{x_1}, \dots, p_{x_n})$ with an equilibrium point of center \times center $\times \dots \times$ saddle type, usually named as “saddle” type. At this point, we use the Poincaré-Birkhoff normalization procedure to perform, in the neighborhood of the saddle, a local sequence of canonical transformations between the original (old) coordinates $(x_1, \dots, x_n, p_{x_1}, \dots, p_{x_n})$ and the normal form (new) coordinates $(q_1, \dots, q_n, p_1, \dots, p_n)$ that lead the Hamiltonian \mathcal{H} to its normal form \mathcal{K} . For more details on normal forms we refer the reader to [20] and references therein. The key feature of this procedure is that, when it is in normal form, the new Hamiltonian is expressed as a function of a set of new n integrals $(J_1, \dots, J_{n-1}, \mathcal{I})$,

$$\mathcal{K} = \mathcal{K}(J_1, \dots, J_{n-1}, \mathcal{I}),$$

where $\mathcal{I} = (p_n^2 - q_n^2)/2$ and $J_i = (p_i^2 + q_i^2)/2$, $i = 1, \dots, n-1$. In the language of reaction dynamics, (q_n, p_n) are the so-called reaction coordinates while the remaining ones are referred to as bath coordinates. Once the normal form is computed to the desired degree of accuracy, in the neighborhood of the saddle point the dynamics takes place on the $(2n-1)$ -dimensional energy surface given by \mathcal{K} . In the normal form coordinates, the Hamilton equations of motion take the following form:

$$\dot{q}_i = \frac{\partial \mathcal{K}}{\partial J_i}(J_1, \dots, J_{n-1}, \mathcal{I}) p_i, \quad i = 1, \dots, n-1,$$

$$\dot{p}_i = -\frac{\partial \mathcal{K}}{\partial J_i}(J_1, \dots, J_{n-1}, \mathcal{I}) q_i, \quad i = 1, \dots, n-1,$$

$$\dot{q}_n = \frac{\partial \mathcal{K}}{\partial \mathcal{I}}(J_1, \dots, J_{n-1}, \mathcal{I}) p_n,$$

$$\dot{p}_n = \frac{\partial \mathcal{K}}{\partial \mathcal{I}}(J_1, \dots, J_{n-1}, \mathcal{I}) q_n. \quad (12)$$

From Eq. (12) it is clear that $q_n = p_n = 0$ and $\mathcal{K} = \text{const}$ is a $(2n-3)$ -dimensional invariant manifold. Moreover, it is a normally hyperbolic invariant manifold (NHIM) [21]. Normal hyperbolicity means that, under the linearized dynamics, the growth and decay rates of tangent vectors normal to the manifold (the “reaction”) dominate the growth and decay of the tangent vectors tangent to the manifold. In this way, a NHIM acts like a higher-dimensional saddle point.

The NHIM is the limit (“equator”) of a $(2n-2)$ -dimensional sphere obtained by setting $q_n = 0$ and $\mathcal{K} = \text{const}$. This $(2n-2)$ -dimensional sphere is the TS. The TS is locally a surface of no return: when a trajectory crosses the TS, it must leave before it (possibly) later reintersects the TS [13]. The NHIM divides the TS in two hemispheres with $p_n < 0$ and $p_n > 0$. The half with $p_n > 0$ ($p_n < 0$) is always crossed by forward (backward) reactive trajectories.

Because the NHIM is unstable in nature, it has attached stable \mathcal{W}^s and unstable \mathcal{W}^u manifolds which act like multi-dimensional separatrices. These surfaces are $(2n-2)$ -dimensional spherical cylinders given by setting, respectively, $p_n = -q_n$ and $p_n = q_n$ in \mathcal{K} . Note that \mathcal{W}^s and \mathcal{W}^u have the right dimensionality to divide the energy shell and thence they are impenetrable barriers in phase space [14] that separate reactive from nonreactive trajectories. Hence the $(2n-2)$ -dimensional stable and unstable surfaces bound a region in the $(2n-1)$ -dimensional energy surface \mathcal{K} that is divided into two components by the TS. All reacting trajectories start in one component, cross the TS, and enter the other component.

At this point, we apply the PSTST to our problem following six steps.

(i) We fix in Hamiltonian (2) a given value of f and then we find numerically the saddle equilibrium point $P_s = (\rho_s, z_s, P_{\rho_s}, P_{z_s}) = (0, z_s, 0, 0)$. This equilibrium is of center \times saddle type and the PSTST applies.

(ii) By means of a translation we move P_s to the origin. Then, the Hamiltonian (2) reads

$$\begin{aligned} \mathcal{H} = & \frac{1}{2}(P_{\rho}^2 + P_z^2) - \frac{1}{\sqrt{\rho^2 + (z + z_s)^2}} + \frac{1}{\sqrt{\rho^2 + (z + z_s + 2)^2}} \\ & - \frac{1}{4(z + z_s + 1)} + f(z + z_s). \end{aligned} \quad (13)$$

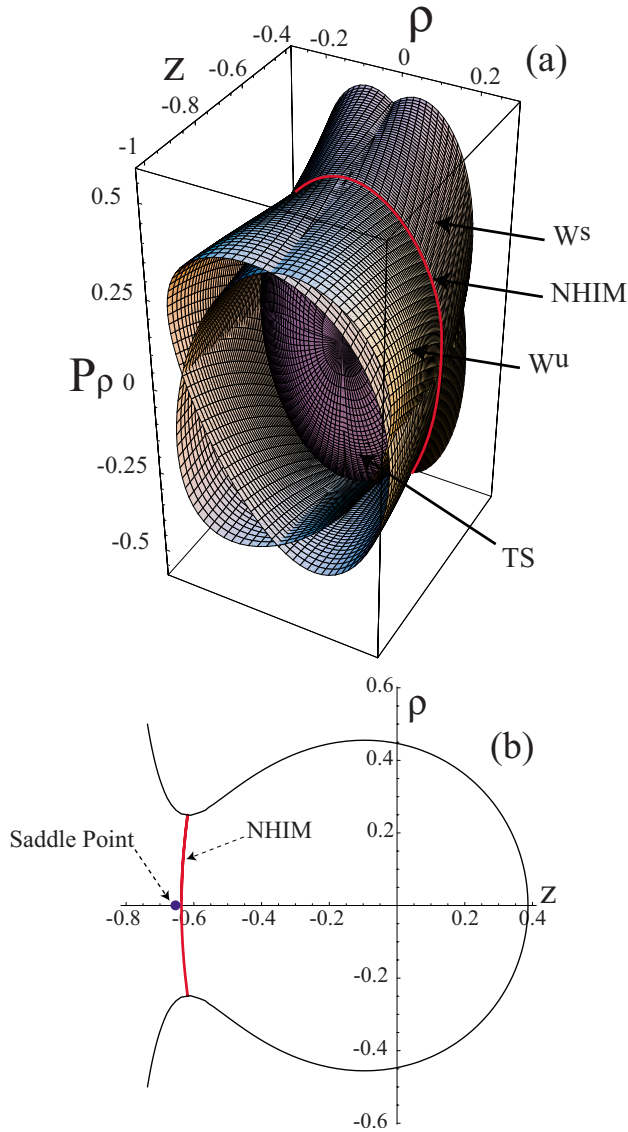


FIG. 7. (Color online) For $\mathcal{E}=-2$ and $f=0.9$, projections in the original coordinates of the NHIM, the transition state TS, and the stable and unstable manifolds W^s and W^u .

(iii) In order to prepare the above Hamiltonian for transformation into normal form, we perform a Taylor expansion of Eq. (13) around the saddle point P_s .

(iv) By using the symbolic manipulator MATHEMATICA, we compute the normal form \mathcal{K} of the expanded Hamiltonian up to degree 14. At this point it is important to understand that \mathcal{K} is expressed as a function of the normal form coordinates denoted as $(\rho_N, z_N, P_{\rho_N}, P_{z_N})$ and that \mathcal{K} is integrable because the quantities $J=(P_{\rho_N}^2 + \rho_N^2)/2$ and $\mathcal{I}=(P_{z_N}^2 - z_N^2)/2$ are the new (approximate) integrals. Then, the normal form is expressed as

$$\mathcal{K} = \mathcal{K}(J, \mathcal{I}) = \sum_{i=1}^N \mathcal{K}_i(J, \mathcal{I}),$$

where \mathcal{K}_i are homogeneous polynomials of degree i in J and \mathcal{I} .

(v) Once the normal form is computed, we obtain the NHIM, the TS, \mathcal{W}^s , and \mathcal{W}^u by setting in \mathcal{K} , respectively, $J=0$, $z_N=0$, $P_{z_N}=-z_N$, and $P_{z_N}=z_N$. The TS half with $P_{z_N} > 0$ is the capture half TS_c , while the one with $P_{z_N} < 0$ is the escape half TS_e .

(vi) Due to the fact that the normal form provides the direct and inverse transformations between the normal form coordinates and the original coordinates, we have the expressions of the coordinates (ρ, z, P_ρ, P_z) as a function of the coordinates $(\rho_N, z_N, P_{\rho_N}, P_{z_N})$. By introducing in these (inverse) transformations the above conditions $J=0$, $z_N=0$, $P_{z_N}=-z_N$, and $P_{z_N}=z_N$, we have the parametric expressions of the NHIM, the transition state, and the stable and unstable manifolds in the original coordinates (ρ, z, P_ρ, P_z) . These expressions can be used, among other things, to visualize these structures.

In particular, from a normal form calculated for $\mathcal{E}=-2$ and $f=0.9$, projections in the original coordinates of these four structures are shown in Fig. 7(a). We note that, because our system has two degrees of freedom, the NHIM is a periodic orbit whose projection onto the configuration space bridges the corresponding equipotential [see Fig. 7(b)].

V. IONIZATION PROBABILITY

In this section we compute the ionization probability by means of a procedure that combines the phase space transition state and a classical spectral theorem. This procedure has been recently developed by Waalkens *et al.* [22] and its main feature is that it is computationally much more efficient than the standard brute-force Monte Carlo sampling method.

For fixed values of the energy \mathcal{E} and the electric field f , according to that procedure, we calculate the ionization probability as

$$P = \frac{V_e}{V_o},$$

that is, the fraction of the energy surface volume V_e of initial conditions in the neighborhood of the hydrogen atom in phase space which leads to escape, over the total energy surface volume V_o of the atom neighborhood in phase space. We consider as atom neighborhood the phase space volume limited by the zero velocity curve for the energy \mathcal{E} under consideration and the escape half TS_e .

In order to calculate the volume V_e , we make use of the classical spectral theorem shown by Pollak [15] in the context of bimolecular collisions, and conjectured by Brumer *et al.* [23]. This theorem states that the volume swept out in

TABLE I. Results for the average passage time $\langle t \rangle$ through the atom neighborhood, the flux ϕ_{TS_e} through TS_c , the energy surface volumes V_e and V_o , and the ionization probabilities $P=V_e/V_o$ and P_∞ obtained with both procedures.

f	$\langle t \rangle$	ϕ_{TS_e}	V_e	V_o	$P=V_e/V_o$	P_∞
0.9	2.93	0.34	1	8.99	0.11	0.12
1	2.88	0.57	1.64	9.07	0.18	0.18

phase space by a set of classical trajectories is the integral of the passage time, that is, the amount of time spent by the set of trajectories in that phase space volume. According to this theorem, if we chose the initial conditions of the set of trajectories in the capture half of the transition state, TS_c , the volume V_e would be given by

$$V_e = \int_{TS_c} t d\rho_N dP_{\rho_N}.$$

Now, if we define the average passage time $\langle t \rangle$ that these trajectories spend in the atom neighborhood until they reach the escape half TS_e as

$$\langle t \rangle = \frac{\int_{TS_c} t d\rho_N dP_{\rho_N}}{\int_{TS_c} d\rho_N dP_{\rho_N}},$$

the volume V_e can be written in this form,

$$V_e = \langle t \rangle \int_{TS_c} d\rho_N dP_{\rho_N} = \langle t \rangle \phi_{TS_c},$$

ϕ_{TS_c} being the flux through the TS_c . Taking into account the Stokes theorem, ϕ_{TS_c} can be directly computed as the action of the NHIM,

$$\phi_{TS_c} = \oint_{NHIM} d\rho_N dP_{\rho_N} = 2\pi J,$$

where J is readily obtained from the normal form \mathcal{K} by solving the equation $\mathcal{K} = \mathcal{K}(J, 0) = \mathcal{E}$.

The total energy surface volume V_o of the atom neighborhood in phase space is calculated by means of the following Monte Carlo sampling procedure. After choosing a hypercube in phase space containing the complete atom neighborhood, we uniformly sample initial conditions inside the hypercube. Then we check whether the corresponding point lies inside the atom neighborhood. Therefore the total energy surface volume V_o is given by

$$V_o = \frac{n_{in}}{n_t} V_{hcube},$$

with V_{hcube} being the volume of the hypercube, n_t the total number of sampled initial conditions, and n_{in} the number of initial conditions inside the atom neighborhood.

In Table I, we show the results obtained with this procedure for two values of the electric field f , and for a fixed energy $\mathcal{E} = -2$. The average time $\langle t \rangle$ has been numerically calculated by choosing about 125 000 initial conditions uniformly distributed on the TS_c and then averaging the corresponding passage times. We have computed a converged value of V_o with samples of about $n_t \approx 10^8$. As it was expected, the average passage time $\langle t \rangle$ that ionization trajectories spend in the atom neighborhood decreases with f , whereas the flux ϕ_{TS_c} , the volume V_e , and the ionization

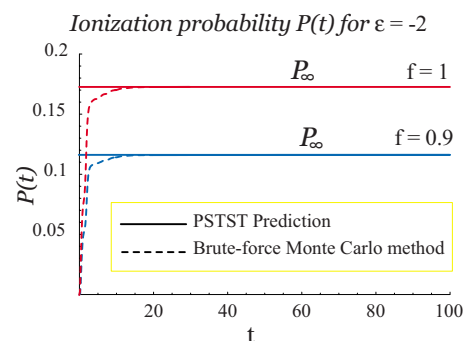


FIG. 8. (Color online) Ionization probability curves P_t obtained with the Monte Carlo sampling method for a uniform distribution of initial conditions in the atom neighborhood for two different values of the scaled electric field f . The horizontal lines represent the corresponding values provided by the alternative method which combines the classical spectral theorem and the PSTST theory.

probability $P = V_e/V_o$ increase with f . These results are in qualitative agreement with the evolution of the Poincaré surfaces of section in Fig. 6.

In order to compare these results with those provided by the standard time-consuming brute-force Monte Carlo procedure, we have sampled initial conditions in the atom neighborhood in phase space with the same value of energy $\mathcal{E} = -2$. Then we have integrated the Hamilton equations of motion until they reach either the TS_e or a large fixed cutoff time $t_{\text{cutoff}} = 500$. This cutoff time has been chosen in such a way that ionization for $t > t_{\text{cutoff}}$ is very unlikely. In Fig. 8 we show the ionization probability curves $P(t)$ versus time t for both values of f . The ionization probabilities saturate for $t \rightarrow \infty$ at values which depend on the energy and f . These saturation values P_∞ should coincide with the ionization probabilities $P = V_e/V_o$ calculated with the previous procedure. For this comparison, Fig. 8 shows as horizontal lines the values of $P = V_e/V_o$ for the corresponding values of f . In the last column of the table, we also show the saturation values of P_∞ obtained with the brute-force method. As it can be seen, the agreement between the results of both procedures is very good.

It is worth noting that the method based on the classical spectral theorem and the PSTST is computationally much more efficient than the standard brute-force Monte Carlo sampling procedures. In fact, for this problem, the efficiency ratio is roughly much more than 1:1000 for a cutoff time of 500 used in the brute-force method.

VI. CONCLUSIONS

In the present work, we have studied the classical dynamics of a hydrogen atom near a metallic surface in the presence of a uniform electric field normal to the surface. Due to the large size of a Rydberg atom, the interaction with the metallic surface takes place relatively far from the surface. Therefore we have used a simple electrostatic image model to describe the atom-surface interaction. Owing to the axial symmetry of the system, the z component P_ϕ of the angular momentum is conserved, and hence the system, expressed in

cylindrical coordinates has two degrees of freedom. After scaling coordinates and momenta, the Hamiltonian depends only on two parameters: the scaled energy \mathcal{E} and the electric field strength f . We have restricted our study to the case $P_\phi=0$.

By means of numerical continuation of families of periodic orbits and Poincaré surfaces of section, we have extensively explored the structure and evolution of the system phase space as a function of the electric field strength f . We have found that, as f increases, the atom is strongly polarized through two consecutive pitchfork bifurcations, reaching a Stark-like regime where the electron orbits are mainly oriented normally to the metallic surface. This classical Stark behavior has its quantum confirmation [5,6] with the localization of wave functions in the vicinity of the polarized classical electron periodic orbits.

The ionization dynamics of the atom has been also investigated by means of the phase space transition state theory (PSTST). We have calculated the ionization probability as a

function of f making use of a recently developed procedure that combines the PSTST and a classical spectral theorem. It is worth noting that this method is computationally much more efficient than the standard time-consuming brute-force Monte Carlo sampling procedures. The results of the ionization probabilities we have computed with both procedures are in very good agreement, as it can be seen in Table I. Moreover, these results are also in qualitative agreement with the evolution of the structure of the Poincaré surfaces of section as f increases for energies bigger than the electron escape energy \mathcal{E}_s .

ACKNOWLEDGMENTS

This work is included in the framework of the research project MTM2005-08595 supported by the Spanish Ministry of Education and Science. The authors wish to thank Dr. Fernando Blesa for his helpful assistance in the use of the numerical software AUTO.

-
- [1] C. Lemell, H. P. Winter, F. Aumayr, J. Burgdörfer, and F. Meyer, *Phys. Rev. A* **53**, 880 (1996); P. Nordlander and J. Modisette, *Prog. Surf. Sci.* **53**, 265 (1996); S. A. Deutscher, X. Yang, and J. Burgdörfer, *Phys. Rev. A* **55**, 466 (1997); P. Kürpick, U. Thumm, and U. Wille, *ibid.* **56**, 543 (1997); U. Thumm, P. Kürpick, and U. Wille, *Phys. Rev. B* **61**, 3067 (2000).
- [2] P. Nordlander, *Phys. Rev. B* **53**, 4125 (1996).
- [3] F. B. Dunning, H. R. Dunham, C. Oubre, and P. Nordlander, *Nucl. Instrum. Methods Phys. Res. B* **203**, 69 (2003).
- [4] P. Nordlander and F. B. Dunning, *Phys. Rev. B* **53**, 8083 (1996).
- [5] J. Hanssen, C. F. Martin, and P. Nordlander, *Surf. Sci.* **423**, L271 (1999).
- [6] Z. Zhou, C. Oubre, S. B. Hill, P. Nordlander, and F. B. Dunning, *Nucl. Instrum. Methods Phys. Res. B* **193**, 403 (2002).
- [7] S. B. Hill, C. B. Haich, Z. Zhou, P. Nordlander, and F. B. Dunning, *Phys. Rev. Lett.* **85**, 5444 (2000).
- [8] C. Oubre, P. Nordlander, and F. B. Dunning, *J. Phys. Chem. B* **106**, 8338 (2002).
- [9] H. Friedrich and D. Wintgen, *Phys. Rep.* **183**, 37 (1989).
- [10] M. Gutzwiller, *Chaos in Classical and Quantum Mechanics* (Springer-Verlag, New York, 1990); T. Uzer, D. Farrelly, J. Z. Milligan, P. E. Raines, and J. P. Skelton, *Science* **253**, 42 (1991).
- [11] P. Kürpick, U. Thumm, and U. Wille, *Phys. Rev. A* **57**, 1920 (1998).
- [12] K. Ganesan and K. T. Taylor, *J. Phys. B* **29**, 1293 (1996).
- [13] T. Uzer, C. Jaffé, J. Palacián, P. Yanguas, and S. Wiggins, *Nonlinearity* **15**, 957 (2002); C. Jaffé, S. Kawai, J. Palacián, P. Yanguas, and T. Uzer, *Adv. Chem. Phys.* **130**, 171 (2005); L. Wiesenfeld, *ibid.* **130**, 217 (2005).
- [14] S. Wiggins, L. Wiesenfeld, C. Jaffé, and T. Uzer, *Phys. Rev. Lett.* **86**, 5478 (2001); H. Waalkens, A. Burbanks, and S. Wiggins, *J. Chem. Phys.* **121**, 6207 (2004).
- [15] E. Pollak, *J. Chem. Phys.* **74**, 6763 (1981).
- [16] F. J. Muñoz-Almaraz, E. Freire, J. Galán, E. Doedel, and A. Vanderbauwhede, *Physica D* **181**, 1 (2003).
- [17] T. Levi-Civita, *Sur la Résolution Qualitative du Problème des Trois Corps* (University of Bologna Press, Bologna, 1956), Vol. 2; E. L. Stiefel and G. Scheifele, *Linear and Regular Celestial Mechanics* (Springer-Verlag, Berlin, 1971).
- [18] N. S. Simonovic, *J. Phys. B* **30**, L613 (1997).
- [19] P. Pechukas, *Dynamics of Molecular Collisions*, edited by W. H. Miller (Plenum, New York, 1976); B. E. Pollak, *Theory of Chemical Reactions Dynamics*, edited by M. Baer (CRC Press, Boca Raton, FL, 1985).
- [20] V. I. Arnol'd, V. V. Kozlov, and A. I. Neishtadt, *Mathematical Aspects of Classical and Celestial Mechanics* (Springer-Verlag, Berlin, 2006); J. Palacián and P. Yanguas, *Nonlinearity* **13**, 1021 (2000).
- [21] S. Wiggins, *Normally Hyperbolic Invariant Manifolds in Dynamical Systems* (Springer-Verlag, New York, 1994).
- [22] H. Waalkens, A. Burbanks, and S. Wiggins, *Mon. Not. R. Astron. Soc.* **361**, 763 (2005); *J. Phys. A* **38**, L759 (2005); *Phys. Rev. Lett.* **95**, 084301 (2005).
- [23] P. Brumer, D. E. Fitz, and D. Wardlaw, *J. Chem. Phys.* **72**, 386 (1980).